International Research Journal of Engineering and Technology (IRJET) e-ISSN: 2395-0056
Volume: 12 Issue: 03 | Mar 2025 www.irjet.net p-ISSN: 2395-0072

Effect of Rice Husk Ash and Silica Fume Dosage on Compressive Strength of Cement Mortar under Varying Curing Ages

Shilong Wang[1], Haoyi Ren[2]

[1,2] *School of Civil Engineering and Architecture, Anhui University of Science and Technology, Anhui, China*

Abstract - *This study systematically investigates the effects of rice husk ash (RHA, 0-10%) and silica fume (SF, 0-10%) dosages combined with curing ages (1/14/28 days) on the mechanical properties of cement mortar. Compressive strength tests were conducted using a WAW-1000 computer-controlled electro-hydraulic servo universal testing machine, coupled with scanning electron microscopy (SEM) analysis to reveal the synergistic mechanisms between admixture proportions and curing duration. Results indicate that the 28-day compressive strength of specimens with 5% RHA and 5% SF reaches 48.7 MPa, demonstrating significant improvement compared to the control group. SEM observations confirm densified C-S-H gel formation and reduced porosity in the interfacial transition zone (ITZ) under this optimal mix proportion. The study concludes that cement mortar achieves peak mechanical performance when incorporating 5% RHA and 5% SF with 28-day curing. These findings provide theoretical insights for the mix design and age-dependent behavior prediction of agricultural waste-based green mortars.*

Key Words: Dosage, Age, Rice husk ash, Cement mortar, Compressive strength.

1. INTRODUCTION

As the world's largest rice producer, China generates over 40 million tons of rice husk waste annually. The improper disposal methods such as open-air burning and random stockpiling have led to severe environmental challenges, including particulate pollution and greenhouse gas emissions. Since the 1980s, Chinese researchers have systematically explored the resource utilization of rice husk ash (RHA), achieving groundbreaking progress: A Tsinghua University research team first validated the feasibility of RHA as a siliceous admixture (1985), the China Building Materials Academy developed a calcination activation process for RHA that was granted a national patent (1992), and engineering applications in modified high-iron Sulphoaluminate cement have been realized over the past decade. However, critical limitations persist in current studies: [1] RHA applications remain predominantly confined to single-sector construction materials, with insufficient investigation into its synergistic effects with industrial by-products like silica fume (SF); [2] The coupling mechanisms between dosage and curing age variables lack clarity, constrained by inadequate long-term performance evolution data; [3] The cross-scale correlation between microstructural optimization and macroscopic mechanical responses requires further exploration.

The cement industry, contributing significantly to global carbon emissions, demands sustainable technologies for green transition. While silica fume (SF) has been widely adopted to enhance mechanical properties of cementitious materials due to its high pozzolanic activity, its high production costs and limited availability hinder large-scale applications. Conversely, rice husk ash (RHA), a silica-rich agricultural by-product, demonstrates promising substitution potential.

This study designs experimental protocols to systematically investigate the effects of dual incorporation parameters of RHA and SF on the compressive strength of cement mortar under curing ages of 1/14/28 days. The findings aim to provide practical methodologies for agricultural waste valorisation and cementitious material design, thereby advancing the circular economy in the construction sector.

2. Experimental Design

The materials used in this study included rice husk ash (RHA) calcined at 600°C, 42.5-grade ordinary Portland cement, sand with a fineness modulus of 1.69, and silica fume (SF) containing 96% SiO_2. Tap water was employed for both mixing and curing processes. The RHA preparation began with soaking raw rice husks in a hydrochloric acid solution under continuous stirring for 1 hour. After acid treatment, the husks were thoroughly rinsed with distilled water to achieve a neutral pH. The cleaned husks were then dried in an oven and subsequently calcined in a muffle furnace at 600°C for 3 hours. Following calcination, the RHA was rapidly quenched in an ice-water mixture (0°C), dried again, and ground into a fine powder passing through a 180-mesh sieve.

The mix proportions were designed based on previous research [4-6], with a cement: sand: water ratio of 330:1210:160 kg/m^3. Six distinct mix groups (labelled G1 to G6) were prepared by replacing SF with RHA at substitution rates of 0%, 10%, 30%, 50%, 70%, and 90%, respectively. All specimens were fabricated and cured in compliance with the Standard for Test Methods of

Mechanical Properties of Ordinary Concrete (GB/T 50081-2002).

The experimental procedure emphasized rigorous control of material preparation and mixing protocols to ensure consistency. Mechanical mixing was adopted for homogenizing the cement mortar, and specimens were cast into standardized molds. The curing regime adhered to controlled environmental conditions to minimize variability, with subsequent mechanical testing focused on evaluating the compressive strength development across different substitution levels and curing durations. This systematic approach aimed to elucidate the feasibility of RHA-SF synergy in sustainable cementitious materials.

Table -1: Cement mortar ratio

Number	Water	Sand	Cement	Rice husk ash	Silica fume
G1	0.366	4.069	1	0	0.115
G2	0.366	4.069	1	0.012	0.100
G3	0.366	4.069	1	0.034	0.078
G4	0.366	4.069	1	0.056	0.056
G5	0.366	4.069	1	0.078	0.034
G6	0.366	4.069	1	0.100	0.012

In the preparation of cement mortar specimens, cubic mold with size of 70.7 mm × 70.7 mm × 70.7 mm were used. Six groups of specimens with varying mix proportions were cast sequentially, with three replicates per group. After casting, cement mortar specimens were placed in a controlled curing chamber for 1 d, 14 d, and 28 d.

3. Experimental Methods

The static uniaxial compression test was conducted using a WAW-1000 universal testing machine. The test employed displacement-controlled loading at a rate of 0.01 m/s, with a maximum load capacity of 1000 kN. Prior to testing, the load cell was calibrated to zero, and the data acquisition system was initialized. The cross-sectional dimensions of each specimen were measured using a vernier caliper. Specimens were centrally aligned on the compression plates. During testing, the load was applied uniformly until failure, with the yield load and ultimate failure load recorded. Post-test, stress-strain curves were plotted based on the experimental data.

A FlexSEM1000 scanning electron microscope was utilized for microstructural analysis. The instrument was activated and purged with inert gas to stabilize the system. Pre-treated specimens were mounted on the stage, and the chamber was evacuated to achieve a high vacuum. Microstructural images were captured at magnifications relevant to interfacial transition zone (ITZ) and hydration product characterization.

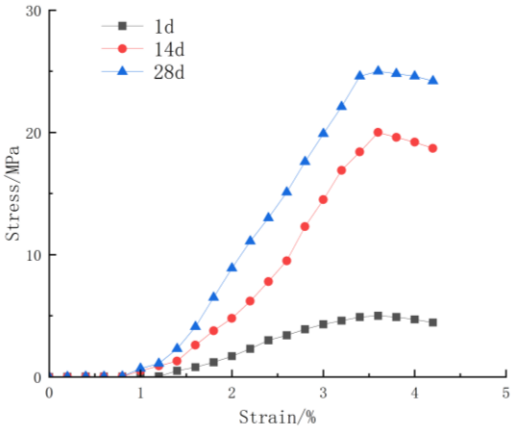

Fig -1: Stress-strain curves under different curing ages

Fig 1 illustrates the stress-strain curves of Group G1 specimens at varying curing ages. All curves exhibit a single-peak pattern and undergo four distinct phases: compaction stage, elastic deformation stage, crack propagation stage, and failure stage.

During the compaction stage, the stress increases gradually with strain. Notably, the duration of this phase shortens as curing age progresses. In the elastic deformation stage, minor external loading induces elastic deformation within the cement mortar, while internal microcracks and pores develop slowly. A linear proportionality between stress and strain is observed in this regime.

As external load intensifies in the crack propagation stage, visible cracks initiate and expand. The slope of the stress-strain curve increases with curing age, accompanied by a corresponding rise in peak stress at failure. During the failure stage, cracks extend, interconnect, and coalesce, ultimately leading to specimen disintegration. Comparative analysis reveals that prolonged curing ages enhance material stiffness and delay crack initiation, attributed to improved hydration and interfacial bonding.

3.1 Compressive Strength Analysis of Specimens at Different Ages

The uniaxial compressive strength of cement mortar is one of the important mechanical indexes, and it can be calculated as follows.

$$\sigma_c = \frac{P}{A}$$

Where σ_c is the uniaxial compressive strength, P is the axial load, and A is the cross-sectional area of the specimen.

According to the formula, a uniaxial compression test was conducted on rice husk ash and silica fume cement mortar at different ages, and the relationship between compressive strength and curing age was shown in the figure.

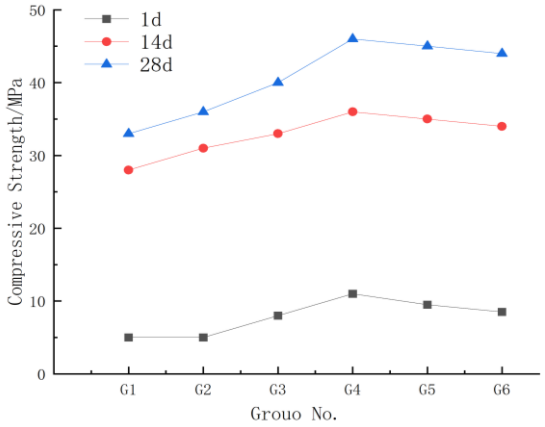

Fig -2 : Compressive strength of specimens at different ages

Fig 2 shows the relationship between compressive strength and curing age of cement mortar specimens. When the curing age is not more than 14 days, the compressive strength of G2 group is lower than G1, which indicates that the early strength of mono-doped silica fume cement mortar is low. At this time, the compressive strength of G2 group specimens at 1d, 14d and 28d was 5.01MPa, 31.08MPa and 36.32MPa, respectively. This is because the specimens are jointly affected by the pozzolanic effect of silica fume, the micro-aggregate filling effect and the dilution effect on cement [7]. When the cement mortar specimen was cured within 14 days, the pozzolanic effect of the silica fume was not fully brought into play, and the dilution effect of the cement caused by the addition of silica fume made its strength lower than that of the control group without the addition of silica fume. Except for the control group (G1), the compressive strength of the samples increased first and then decreased with the increase of the replacement ratio of rice husk ash. With the increase of age, the compressive strength of rice husk ash and wolcrete cement mortar with different content increases gradually. When the replacement ratio of rice husk ash reaches 50%(G4), the compressive strength of specimens at different ages reaches the highest. At this time, the compressive strength of 1d, 14d and 28d was 11.55MPa, 36.91MPa and 48.7MPa, respectively. It can be seen that the combined action of rice husk ash and silica fume can obviously improve the compressive strength of cement mortar.

According to the above analysis, it can be concluded that the greater the peak stress, the shorter the interval of the compaction section and the larger the slope of the failure stage curve, which reflects the brittleness characteristics. Moreover, the addition of rice husk ash and silica fume makes the failure of cement mortar ductile. The compressive strength increases with the increase of age. With the increase of the proportion of rice husk ash instead of silica fume, the compressive strength of cement mortar showed a trend of first increasing and then decreasing. When the replacement ratio of rice husk ash reaches 50%(G4), the compressive strength of specimens at different ages reaches the highest.

3.2 Failure mode analysis of specimens

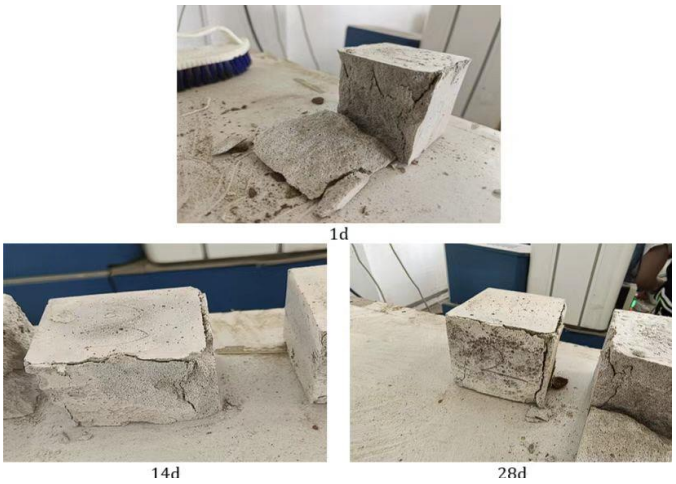

Fig -3 Failure Modes of Specimens

Fig. 3 shows the failure mode of the specimen. With the increase of curing age, the failure degree of the specimen decreases, which is a manifestation of brittle failure characteristics.

Fig-4 : Failure Modes of Specimens with Varying RHA-SF Substitution Ratios

As illustrated in Fig 4, the damage morphology of specimens with varying RHA-SF substitution ratios is compared. The control group exhibited the most severe damage morphology, characterized by extensive crack propagation and pronounced fragmentation. A non-linear trend in failure severity was observed with increasing RHA substitution: initial reductions in crack density and fragmentation occurred at low-to-moderate substitution levels, followed by intensified damage at higher substitutions.

At a 50% rice husk ash substitution ratio (Group G4), specimens exhibited minimal fragmentation under external loading, with localized spalling at both ends and no visible cracks in the central region. However, deviations from this optimal substitution ratio (either higher or lower RHA content) progressively intensified damage severity. Increased substitution levels exacerbated end spalling and promoted crack propagation in the central zone, accompanied by elevated crack density.

4. MICROSTRUCTURAL ANALYSIS

To analyze the internal microstructure of RHA-silica fume (SF) blended cement mortars under varying substitution ratios and freeze-thaw cycles, fragments from fractured specimens were immersed in ethanol for 24 hours to terminate hydration. The samples were then oven-dried at 60°C for 24 hours, sputter-coated with gold to enhance conductivity, and examined using a FlexSEM1000 scanning electron microscope under high vacuum conditions.

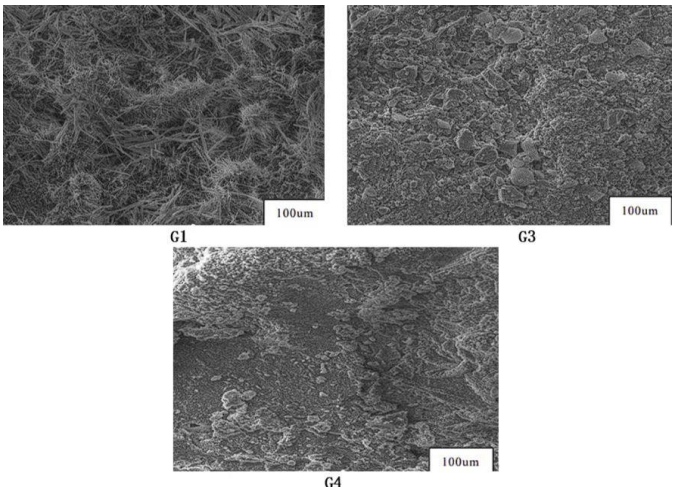

Fig -5 : Microstructural Image of Rice Husk Ash and Silica Ash Mortar at Different Dosage and Same Age(28d)

As shown in Figure 5, the microstructural morphology of 28-day cured specimens revealed distinct variations with substitution ratios. At 50% RHA substitution (G4), the microstructure demonstrated tightly packed hydration products (e.g., C-S-H gels) with sparse surface flocculation. Deviations from this ratio (either higher or lower RHA content) resulted in progressively looser matrices and increased flocculent deposits.

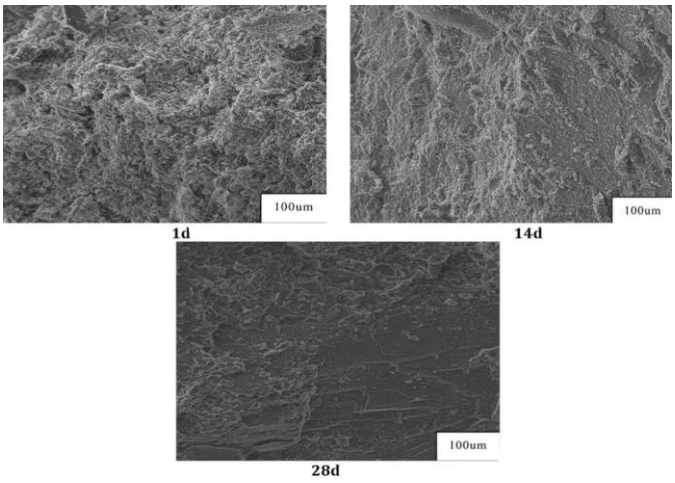

Fig -6: Microstructural images of mortar containing rice husk ash and silica fume at different curing ages with identical additive dosage (G4)."

The evolution of the microstructure of cement mortar is closely correlated with its curing age:

At the early stage (1d), hydration product nucleation dominates [8], characterized by the formation of initial C-S-H gels and ettringite.

At the mid-term stage (14d), pore refinement and interfacial transition zone densification become the primary drivers of performance enhancement [9], as hydration products progressively fill macropores and strengthen the matrix-aggregate interface.

At the long-term stage (28d), environmental impacts (e.g., carbonation, drying shrinkage) may induce micro-damage accumulation in the ITZ, necessitating durability-focused evaluations [10].

Strategic measures, such as adjusting the water-to-cement ratio, incorporating active materials (e.g., fly ash), and optimizing curing regimes, have been demonstrated to suppress harmful pore evolution and enhance interfacial bonding [11]. Future research should integrate multiscale characterization echniques (e.g., SEM-EDS, nanoindentation) to establish quantitative relationships between microstructural parameters and macroscopic properties, thereby advancing durability-oriented design frameworks.

5. CONCLUSION

The results show that rice husk ash can improve the performance of cement mortar and reduce the cost. With the increase of rice husk ash replacement ratio, mortar strength first increased and then decreased. When the

proportion of rice husk ash replacing silica ash was 50%, the strength of specimens at different ages reached the highest value. In addition, the longer the curing time, the more obvious the mortar strength increase.

Through macroscopic and microscopic analysis, it was found that the addition of proper amount of rice husk ash could optimize the material structure and reduce cracks. This method not only saves the amount of silica fume, but also provides a new choice of economic and environmental protection for green buildings. In the future, the performance of materials in freezing and thawing and other extreme environments can be further studied to expand its practical application scenarios.

ACKNOWLEDGEMENT

This work was funded by Anhui Provincial innovation and entrepreneurship training program for college students (No. 202310361107).

REFERENCES

[1] J. Wang, Q. Zhou, Q. Zeng, et al., "Effect of calcination temperature of rice husk ash on the properties of modified cement mortar," Contemporary Chemical Industry, vol. 53, no. 04, 2024, pp. 860-863+868, doi:10.13840/j.cnki.cn21-1457/tq.2024.04.017.

[2] S. Ma, B. Ma, J. Huang, et al., "Influence of rice husk ash as amorphous siliceous material on the structure and properties of fly ash autoclaved aerated concrete," Journal of Wuhan University of Technology, vol. 41, no. 07, 2019, pp. 27-33.

[3] Q. Wang, X. Xie, J. Gao, et al., "Effect of silica fume and rice husk ash on the anti-deterioration properties of bamboo pulp fiber cement-based composites," Concrete and Cement Products, no. 01, 2023, pp. 50-55, doi:10.19761/j.1000-4637.2023.01.050.06.

[4] S. Zhang, D. Huang, B. Yang, et al., "Effect of blast furnace slag content on capillary pore structure of concrete under different water-cement ratios and curing ages," Journal of Jinling Institute of Technology, vol. 38, no. 01, 2022, pp. 79-84, doi:10.16515/j.cnki.32-1722/n.2022.01.013.

[5] J. Wan, A. Zhu, "Study on the influence of lithium slag on the mechanical properties of cement mortar," Concrete, no. 07, 2022, pp. 130-133.

[6] J. Tang, L. Ning, Z. Zhang, et al., "Research on repeated thermal damage of cement mortar based on low-field nuclear magnetic resonance technology," Bulletin of the Chinese Ceramic Society, vol. 41, no. 10, 2022, pp. 3403-3412, doi:10.16552/j.cnki.issn1001-1625.2022.10.013.

[7] G. Liu, M. Bai, P. Zhao, "Effect of pretreated silica fume on the performance of cement paste and mortar," Non-Metallic Mines, vol. 39, no. 06, 2016, pp. 11-14+19.

[8] B. Li, "Mechanism of Keggin-Al13 in Regulating the Hydration Process and Product Structure of Slag Cement," Ph.D. dissertation, Wuhan University of Technology, 2020, doi:10.27381/d.cnki.gwlgu.2020.000058.

[9] R. Zhao, "Strengthening Mechanism of Defective Aggregates Considering Permeation Path and Crystallization Process, and Concrete Performance," Ph.D. dissertation, Chongqing Jiaotong University, 2024, doi:10.27671/d.cnki.gcjtc.2024.000985.

[10] P. Zhang and Q. Ren, "A Particle Flow Bond Degradation Model for Fatigue Damage Accumulation Analysis of Concrete Under Cyclic Loading," Engineering Mechanics, vol. 38, no. S1, pp. 100–109, 2021.

[11] X. Song, X. Li, S. Xu et al., "Effect of Size on the Bonding Performance of FRP-Reinforced Cement Board and Concrete Interface," Journal of North China University of Technology, vol. 37, no. 01, pp. 13–21, 2025.